Desalination and Water Treatment
www.deswater.com
doi: 10.1080/19443994.2014.922500

55 (2015) 945–955
July

Taylor & Francis
Taylor & Francis Group

Evaluation of a low-phosphorus terpolymer as calcium scales inhibitor in cooling water

Yiyi Chen[a], Yuming Zhou[a,*], Qingzhao Yao[a,*], Yunyun Bu[a], Huchuan Wang[a], Wendao Wu[b], Wei Sun[b]

[a]*School of Chemistry and Chemical Engineering, Southeast University, Nanjing 211189, P.R. China, Tel. +86 25 52090617; emails: chenyiyi0220@126.com (Y. Chen), ymzhou@seu.edu.cn (Y. Zhou), 101006377@seu.edu.cn (Q. Yao), 1067477447@qq.com (Y. Bu), whc03231986@163.com (H. Wang)*
[b]*Jianghai Environmental Protection Co., Ltd., Changzhou, Jiangsu 213116, P.R. China, Tel. +86 25 52090617; emails: 13887303@qq.com (W. Wu), leojhhg@sina.com (W. Sun)*

Received 28 November 2013; Accepted 4 May 2014

ABSTRACT

Scale formation, e.g. precipitation of calcium carbonate and calcium sulfate, is a significant problem in cooling water system. For the control of calcium scale and in response to environmental guidelines, the novel low-phosphorus terpolymer was prepared through free radical polymerization reaction of acrylic acid (AA), oxalic acid-allypolyethoxy carboxylate (APEM), and phosphorous acid (H_3PO_3) in water with redox system of hypophosphorous and ammonium persulfate as initiator. The synthesized AA–APEM–H_3PO_3 terpolymer was characterized by Fourier transform infrared spectrometer (FT-IR) and ^{1}H NMR. The inhibition property of the low-phosphorus terpolymer towards $CaCO_3$ and $CaSO_4$ in the artificial cooling water was studied through static scale inhibition tests, and the effect on morphology of $CaCO_3$ and $CaSO_4$ was investigated with combination of scanning electron microscopy and X-ray powder diffraction analysis, respectively. FT-IR was also used to study the effect on morphology of $CaCO_3$. It was shown that AA–APEM–H_3PO_3 exhibited excellent ability to control calcium scale, with approximately 90.16% $CaCO_3$ inhibition and 96.94% $CaSO_4$ inhibition at levels of 8 and 4 mg/L AA–APEM–H_3PO_3, respectively. AA–APEM–H_3PO_3 also displayed ability to change the morphologies and crystal structures of $CaCO_3$ and $CaSO_4$ precipitates. The proposed inhibition mechanism suggests the surface complexation and chelation between the functional groups –P(O) $(OH)_2$, –COOH, and Ca^{2+}, with polyethylene glycol segments increasing its solubility in water.

Keywords: Low-phosphorous; Terpolymer; Scale inhibition; Calcium carbonate; Calcium sulfate

1. Introduction

One of the main problems of water cooling systems is scaling phenomenon, which has a great impact on economy and technology. Deposit formation may cause severe corrosion, deteriorate conditions of the heat exchange, decreased efficiency, and increased frequency of chemical cleaning [1–4]. The clogging of pipes is the consequence of the scale formation, which leads to the shutdown of an industrial plant in the

*Corresponding authors.

worst cases. Commonly, scales consist of calcium carbonate, calcium sulfate, magnesium hydroxide, barium sulfate, calcium phosphate, calcium oxalate, etc., among which carbonate and sulfate of calcium are considered most frequent in cooling water systems [2,5,6]. Precipitation of these two scales from hard water has been studied for a long time because, in addition of its fundamental interest, it is a very important problem from a practical point of view [1,7].

To mitigate the problem of scale deposition, a number of inhibitors which affect the nucleation rate, crystal growth, precipitated variety, and crystal habit have been widely used in industries to treat cooling water. Akyol et al. and Oner et al. showed that phosphonate additives, polyacrylate, and acidic acrylate (methacrylate) polymers once added in solution in small quantities, delay the precipitation onset and decrease the growth rate. The authors explained the inhibitory power by the adsorption of these additives onto crystal growth sites of nascent crystals, altering their surface properties [8,9]. The main scale inhibitors now applied are phosphates and polycarboxylates [10]. Phosphates, 1-hydroxy ethylidine-1-diphosphonic acid, nitrilotris methylene phosphonic acid, and 1,2-diaminoethanetetrakis-methylene phosphonic acid are potent scale inhibitors, poisoning the crystal growth at concentrations far below stoichiometric amounts of the reactive cations [11–14]. However, these inhibitors contain high phosphorus, which can serve as nutrients leading to eutrophication difficulties. On the other hand, high-phosphonate concentration can create severe problems such as insolubility of phosphonate complexes and increase the potential of formation of calcium–phosphate deposits in the presence of excessive amounts of calcium [15,16]. Polycarboxylic acid, such as polyacrylic acid (PAA), a well-known scale inhibitor, has relatively good performances on calcium carbonate or calcium sulfate scale under conditions of certain range pH, while it can create insolubilization of polymer complexes in the presence of excessive amounts of calcium. Increasing environmental concerns and discharge limitations have caused scale-inhibitor chemistry to move towards "green antiscalant" that readily biodegrade and has low mobility for minimum environmental impact [10,17–19]. As a result, the current trend for inhibitor usage is to develop low phosphorous and phosphorus-free polymers, with wider range of pH and higher calcium tolerance.

In the present study, AA–APEM–H_3PO_3 terpolymer containing low phosphorous was prepared with water as solvent and redox system of hypophosphorous and ammonium persulfate as initiator by the free radical polymerization. The elemental composition of the low-phosphorus terpolymer by energy dispersive X-ray analysis (EDX) showed that phosphorus content was less than 1.5% (mass percentage), so the low-phosphorus terpolymer is a new environmentally safe cooling water treatment agent. The structure of AA–APEM–H_3PO_3 was characterized by Fourier transform infrared (FT-IR) and ^{1}H NMR. The antiscale property of the low-phosphorus terpolymer towards $CaCO_3$ and $CaSO_4$ in the artificial cooling water was studied through static scale inhibition tests, and the mechanism was investigated through determining the morphology and crystal structure by scanning electron microcopy (SEM), X-ray diffractometer (XRD), and FT-IR spectrometer.

There are few reports of low-phosphorus terpolymer of AA–APEM–H_3PO_3 used as a scale inhibitor in cooling water. Because of its low phosphorus and decreasing eutrophication, it is believed to represent a potentially new environmentally safe scale inhibitor suitable for cooling water systems.

2. Experimental section

2.1. Materials

2.1.1. Chemicals and reagents

Calcium chloride, sodium bicarbonate, AA, sodium sulfate, phosphorous acid (H_3PO_3), and ammonium persulfate used were obtained from Zhongdong Chemical Reagent Co., Ltd (Nanjing, Jiangsu, People's Republic of China). All the above chemicals were in analytically pure grade without further purification, unless otherwise specified. Commercial inhibitor of poly (acrylic acid) (1800 M_W) was in technical grade and supplied by Jiangsu Jianghai Chemical Co., Ltd. Deionized water (DI water) was used throughout the experiment.

2.1.2. Preparation of AA–APEM–H_3PO_3 terpolymer

The synthesis procedure of APEM is shown in Fig. 1. APEM was synthesized from allyloxy polyethoxy ether ($APEG_n$) in our laboratory according to H.C. Wang's procedure [20]. AA was copolymerized with APEM and phosphorous acid (H_3PO_3) in aqueous medium. The copolymerization reaction was carried out in a 250 mL round-bottom flask with a mechanical stirrer, thermometer, and reflux condenser. A total of 0.5 mol AA and 40 mL DI water were mixed stirring continuously under nitrogen atmosphere. A definite proportion of APEM and H_3PO_3 were added in 20 mL DI water and heated to the reaction temperature 80°C over a period of time. In fixed conditions, the initiator

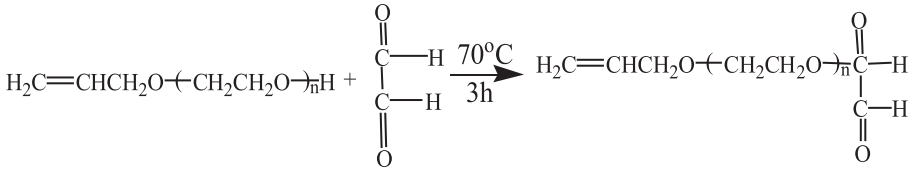

Fig. 1. Synthesis procedure of APEM ($n = 5$, 8, and 12).

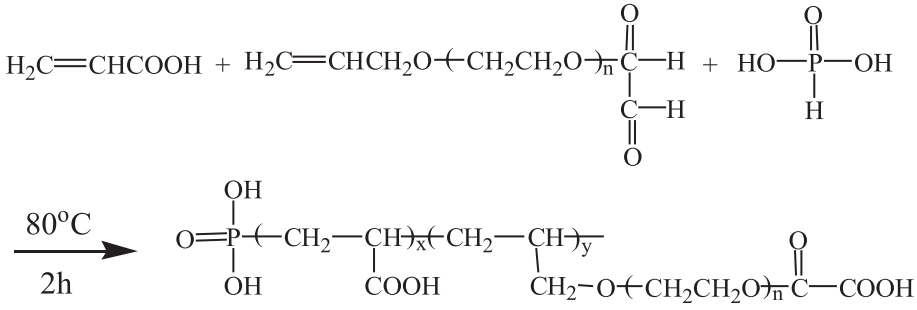

Fig. 2. Synthesis procedure of AA–APEM–H_3PO_3 ($n = 5$, 8, and 12).

ammonium persulfate was dropped at a certain flow rate separately for more than 1 h. Finally, the low-phosphorus terpolymer AA–APEM–H_3PO_3 was obtained, containing about 23.48% solid. The synthesis procedure of the terpolymer is displayed in Fig. 2.

2.2. Methods

2.2.1. Characterization of the synthesized AA–APEM–H_3PO_3

Molecular weight determinations were performed by gel permeation chromatography (GPC, calibrated with polyethylene glycol [PEG] standards) with water as the mobile phase at a flow rate of 1.0 mL/min. The structure of AA–APEM–H_3PO_3 terpolymer was analyzed by FT-IR spectroscopy (VECTOR-22, Bruker Co., Germany) between 4,500 and 0 cm^{-1}, which was used to confirm the presence of expected functional groups responsible for the scale inhibition property. One milligram dried AA–APEM–H_3PO_3 was mixed with 100 mg dried KBr powder and then compressed into a disk for spectrum recording. A Bruker NMR analyzer (AVANCE AV-500, Bruker, Switzerland) was also used to explore the structures of APEG, APEM, and AA–APEM–H_3PO_3, operating at 500 MHz. Thermogravimetric analysis (TGA) was performed using a thermal gravimetric analysis apparatus at a heating rate of 10 K/min in a nitrogen atmosphere with a sample size of 50 mg.

2.2.2. Static scale inhibition tests

The inhibition ability of the low-phosphorus AA–APEM–H_3PO_3 terpolymer for calcium carbonate scale was compared with that of the free inhibitor in flask tests and all inhibitor dosages given below are on a basis of dried conditions [21]. The experiment was carried out in artificial cooling water which was prepared by mixing aqueous solutions of two soluble salts, such as $CaCl_2$ and $NaHCO_3$. Two concentrations of Ca^{2+} and HCO_3^- were 750 mg L^{-1}, according to the national standard of People's Republic of China (GB/T 16632–2008). The artificial cooling water containing different quantities of the low-phosphorus terpolymer was heated at 80°C for 10 h in water bath. After that, it was cooled to room temperature. The remaining Ca^{2+} in the supernatant was titrated by EDTA standard solution and compared with blank test. The inhibition efficiency η was defined as:

$$\eta = \frac{\rho_1(Ca^{2+}) - \rho_1(Ca^{2+})}{\rho_0(Ca^{2+}) - \rho_2(Ca^{2+})} \times 100\%$$

where ρ_0 (Ca^{2+}) was the total concentrations of Ca^{2+} (mg L^{-1}), ρ_1 (Ca^{2+}) was the concentrations of Ca^{2+} (mg L^{-1}) in the presence of the terpolymer inhibitor, and ρ_2 (Ca^{2+}) was the concentrations of Ca^{2+} (mg L^{-1}) in the absence of the terpolymer inhibitor.

Procedure of calcium sulfate precipitation experiments was also carried out similarly to calcium

Table 1
Molecular weight of the polymers

Polymer	AA–APEM–H_3PO_3 ($n = 5$)	AA–APEM–H_3PO_3 ($n = 8$)	AA–APEM–H_3PO_3 ($n = 12$)
Molecular weight (g/mol)	10,397	13,768	17,525

carbonate precipitation experiments, according to the national standard of People's Republic of China concerning the code for the design of industrial oil field–water treatments (SY/T 5673-93). Calcium sulfate was formed from supersaturated solutions prepared by mixing of $CaCl_2$ and Na_2SO_4 solutions, with 2,500 mg L^{-1} Ca^{2+} and SO_4^{2-}. Then the solution was evenly reacted in a water bath at 60℃ for 10 h and the determination of Ca^{2+} was done by exactly same process.

2.2.3. Morphology characterization

The morphological change of the $CaCO_3$ and $CaSO_4$ crystals on glass plates was examined through SEM, XRD, and FT-IR with the addition of the terpolymer. The samples were coated with a layer of gold and observed in a S-3400N HITECH SEM. Precipitated phases were identified by XRD on a Rigaku D/max 2400 X-ray powder diffractometer with Cu Kα ($\lambda = 1.5406$) radiation (40 kV, 120 mA) and an FT-IR spectrophotometer.

3. Results and discussion

3.1. Molecular weight determination

The molecular weight is an important parameter in the process of scale inhibition. The weight distribution of the polymers was investigated with GPC (calibrated with PEG standards) with the 1.0 mL/min run flow rate and the results are listed in Table 1.

3.2. Structure analysis of AA–APEM–H_3PO_3

EDX was performed to get information about the elemental composition of the low-phosphorus AA–APEM–H_3PO_3 terpolymer, including C, O, and P. Above all, the phosphorus content is less than 1.5% in weight, which carried the points of low-phosphorus content and environment friendly.

The FT-IR spectra were taken for the synthesized terpolymer (a), raw materials AA (b), and APEM (c), which are presented in Fig. 3. It is shown that there are characteristic absorption peaks of 2,308, 1,144, 1,012, and 766 cm^{-1}, among which the vibration at 2,308 cm^{-1} is attributed to P–O_{str}, 1,144 and 1,012 cm^{-1}

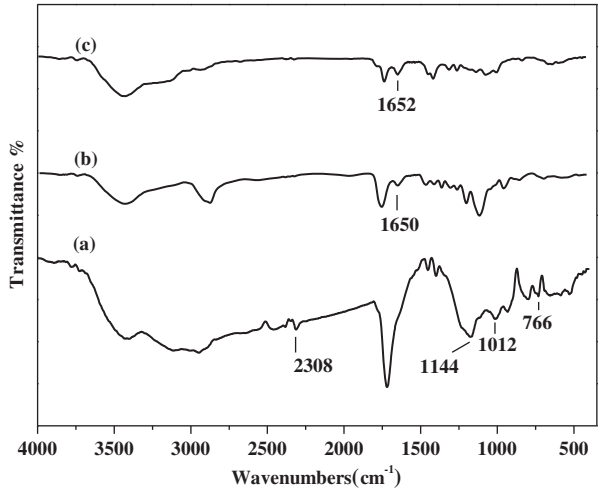

Fig. 3. The FT-IR spectrum of (a) AA–APEM–H_3PO_3 (b) AA (c) APEM.

is attributed to P=O_{str}, and most importantly, 766 cm^{-1} is attributed to P–C_{def} [3,10]. The peaks that appear at 1,650 and 1,652 cm^{-1} are for the C=O stretching vibration, while there are no peaks between 1,620 and 1,680 cm^{-1} in curve (a). This appearance reveals clearly that free radical polymerization among AA, APEM, and H_3PO_3 has happened successfully.

The H^1 NMR spectrum of raw material APEM (a) and the low-phosphorus AA–APEM–H_3PO_3 terpolymer (b) are shown in Fig. 4. The peaks between 4 and 6 ppm are assigned to propenyl protons (CH_2=CH–CH_2–) in curve (a), while there are no peaks in this range in Fig. 4(b). In this case, the double bond absorption peaks completely disappear, revealing that the free radical polymerization among AA and APEM has occurred.

After the analysis from FT-IR and H^1 NMR above, the low-phosphorus terpolymer AA–APEM–H_3PO_3 has been synthesized as expected.

3.3. Thermal stability analysis of the terpolymer

TGA was used to investigate the thermal stability of the terpolymer. The corresponding TGA curve for this polymer is depicted in Fig. 5. The data listed show that degradation of the polymer proceeds in

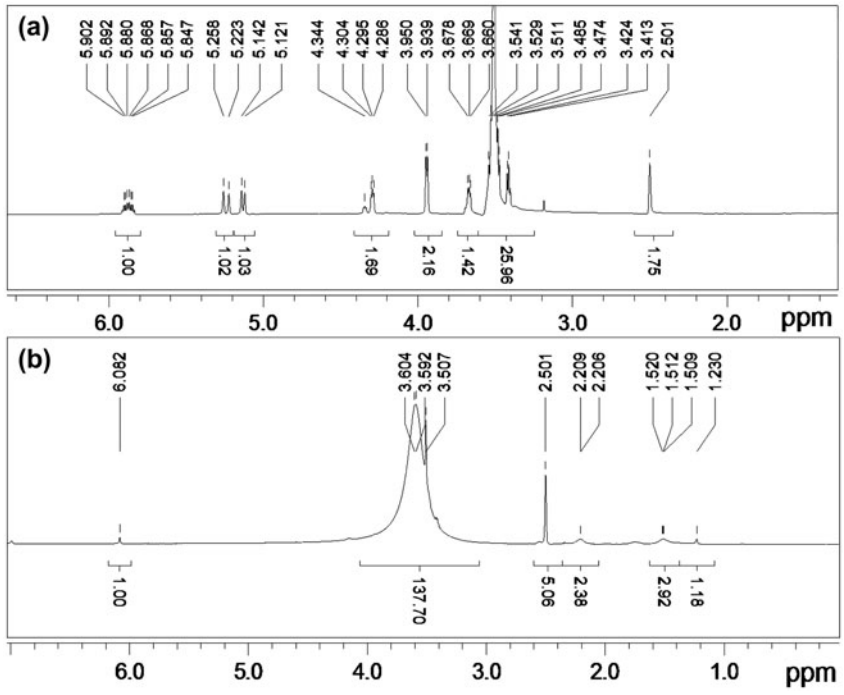

Fig. 4. The H^1 NMR spectrum of (a) APEM and (b) AA–APEM–H_3PO_3.

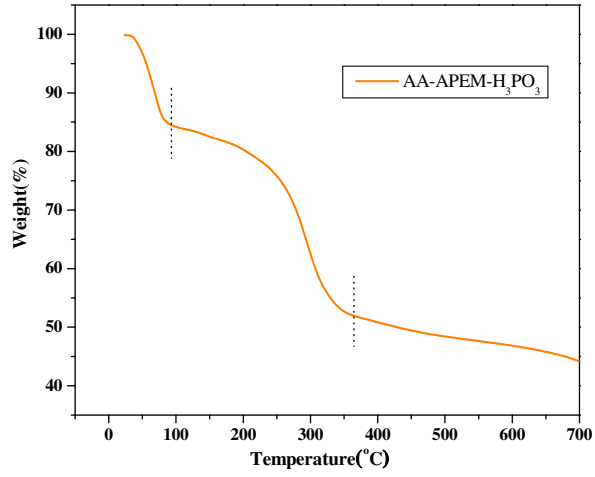

Fig. 5. TGA curve for the polymer.

three stages. It undergoes about 18% weight loss at up to 100°C, which is assigned to the decomposition of active hydroxyl groups (–OH) and evaporation of some water in the polymer. A second stage occurs at 100–400°C, corresponding to the decomposition of carbon–carbon bond, carbon–carbon double bond, and the end-capped carboxylic groups (–COOH) in AA. The last part is attributed to the carbonization of this polymer [22].

3.4. Inhibition property of AA–APEM–H_3PO_3 ($n = 5$, 8, and 12) towards $CaCO_3$ and $CaSO_4$

The inhibitory power of the polymer AA–APEM–H_3PO_3, with different molecular weight, on the formation of calcium carbonate and calcium sulfate precipitation, was compared and shown in Figs. 6 and 7. The data in Fig. 6 show that under the same experimental conditions, and 8 mg/L polymers, the inhibition efficiency obtained for AA–APEM–H_3PO_3 ($n = 12$)

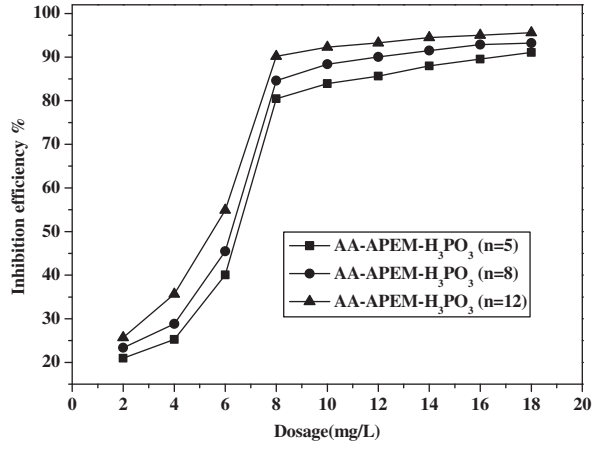

Fig. 6. Scale inhibition of AA–APEM–H_3PO_3 ($n = 5$, 8, and 12) on $CaCO_3$ at different concentrations.

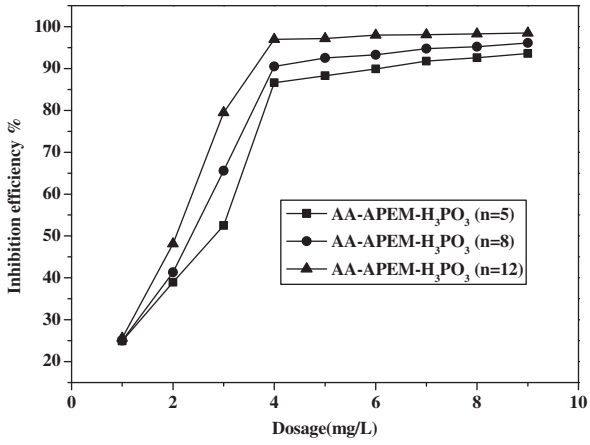

Fig. 7. Scale inhibition of AA–APEM–H_3PO_3 ($n = 5$, 8, and 12) on $CaSO_4$ at different concentrations.

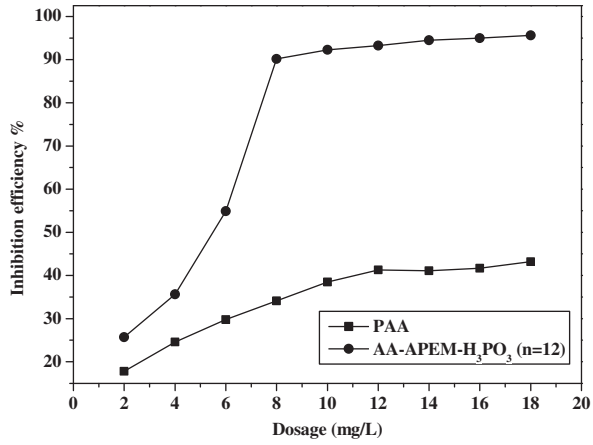

Fig. 8. Inhibition on calcium carbonate as a function of inhibitor dosage ($n = 3$, SD = ±1.580).

is about 90.16%, while it is about 80.5 and 84.7% for AA–APEM–H_3PO_3 ($n = 5$, 8). Fig. 7 illustrates the ability of the terpolymer with different molecular weight to inhibit calcium sulfate under identical conditions. At a level of 4 mg/L, the inhibition value is 96.94% in the presence of AA–APEM–H_3PO_3 ($n = 12$), and it is 86.62 and 90.5% in the presence of AA–APEM–H_3PO_3 ($n = 5$, 8), respectively. Compared to the terpolymer of AA–APEM–H_3PO_3 ($n = 5$) or AA–APEM–H_3PO_3 ($n = 8$), the terpolymer of AA–APEM–H_3PO_3 ($n = 12$) is superior against calcium carbonate and calcium sulfate scale. Therefore, there is a best molecular weight of the terpolymer to obtain the maximum effect for $CaCO_3$ and $CaSO_4$, that is 17,525 ($n = 12$).

The effect of the polymer AA–APEM–H_3PO_3 ($n = 12$), as an inhibitor for calcium carbonate, was compared with that of a conventional polymer, PAA, as shown in Fig. 8. When the terpolymer concentration changes, the inhibition effect also changes correspondingly. That is, scale inhibition effect increases with the increasing concentration of the terpolymer. There is a sudden increase of inhibition efficiency as the concentration increases from 2 to 8 mg/L, which reaches 90.16% at 8 mg/L, from 25.72% at 2 mg/L. Then the terpolymer exhibits an obvious "threshold effect", namely after the concentration exceeds about 8 mg/L, the inhibition efficiency does not obviously increase with the increasing dosages [5]. It is also worth mentioning that PAA, only containing carboxyl groups, can hardly control calcium carbonate scales even at a high dosage, as is apparent from Fig. 8. This fact suggests that the phosphonate groups of phosphorous acid, the side-chain PEG segments of APEM and carboxyl groups of AA might play an important role during the control of calcium carbonate deposits.

Another common precipitation in cooling water system is calcium sulfate, which has caught much attention of academic and industrial researchers [18]. The ability of the low-phosphorus terpolymer to control calcium sulfate deposits, displayed in Fig. 9, was compared with that of PAA, a conventional inhibitor. Different quantities of the low-phosphorus terpolymer and PAA ranging from 1 to 9 mg/L were heated at 60℃ for 10 h. Fig. 9 illustrates the ability of the low-phosphorus terpolymer and PAA under identical conditions. At a level of no more than 2 mg/L, PAA seemed more effective than AA–APEM–H_3PO_3 for calcium sulfate inhibition. However, when the dosage exceeds 2 mg/L, the terpolymer shows great inhibition ability than PAA. The trend is like that of the inhibition property for $CaCO_3$, while the difference is that the inhibition efficiency of $CaSO_4$ reaches 96.94% at a much lower dosage of 4 mg/L.

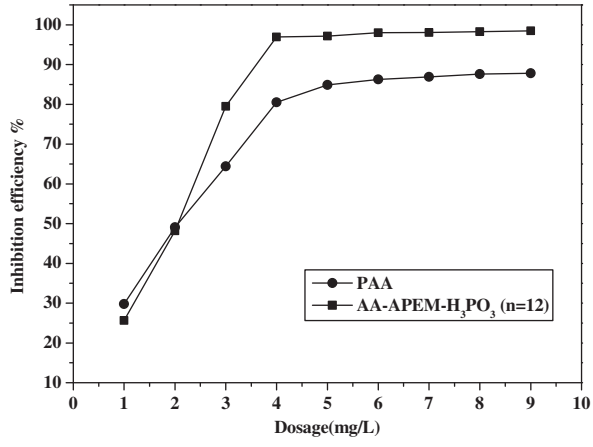

Fig. 9. Inhibition on calcium sulfate as a function of inhibitor dosage ($n = 3$, SD = ±1.648).

3.5. Morphology characterization of calcium scale

3.5.1. SEM analysis of $CaCO_3$ and $CaSO_4$ crystals

SEM is one of the widely used nondestructive surface examination techniques. The change of crystal size and modifications, brought about by the low-phosphorus terpolymer AA–APEM–H_3PO_3 addition, was examined through SEM.

The morphology of the calcium carbonate particles obtained in the absence and presence of 2, 6, and 8 mg/L terpolymer are presented in Fig. 10. Three occurring mineral phases, calcite, aragonite, and vaterite, could be clearly distinguished by their characteristic morphologies [23]. Fig. 10(a) reveals that calcium carbonate scales are mainly calcite scales, which are symmetrical and block like particles of cubic shape or rhombohedral. Variations in the calcite crystal morphology and the crystal sizes are observed in the presence of the low-phosphorus terpolymer AA–APEM–H_3PO_3. Fig. 10(b) illustrates that the well-regulated structure is damaged and it seems that the crystal is split into a great many needles, which is the primary shape feature of aragonite. When the concentration increases to 6 mg/L, oblate spherical shape particles are visible in the SEM image (Fig. 10(c)). There are lots of vaterite phases being more dispersive, which are broken into pieces and set into the bunch crystal with higher concentration. In this case, the deposition will be easily removed with enough shear force from flowing water [24].

The SEM photographs for calcium sulfate scale with and without the presence of the low-phosphorus terpolymer are presented in Fig. 11. It can be seen that the application of the terpolymer in the system (Fig. 11(b)) is an effective way to control the morphology of the calcium sulfate. In Fig. 11(a), regular rod-shaped calcium sulfate tight particles are obtained and look like thin tubular cells and needles exhibiting monoclinic symmetry [5]. With the addition of AA–APEM–H_3PO_3, loose structure, like spongy, with reduced crystallinity is formed. When the concentration of the terpolymer is 2 mg/L, the loose particles became the main part of calcium sulfate. Previously, Amjad [25] studied the effect of polyacrylate on the formation of calcium sulfate scales and claimed that the structure of the crystals is highly modified.

3.5.2. XRD analysis of $CaCO_3$ and $CaSO_4$ crystals

To examine the scale structural changes in calcium carbonate and calcium sulfate in the presence and

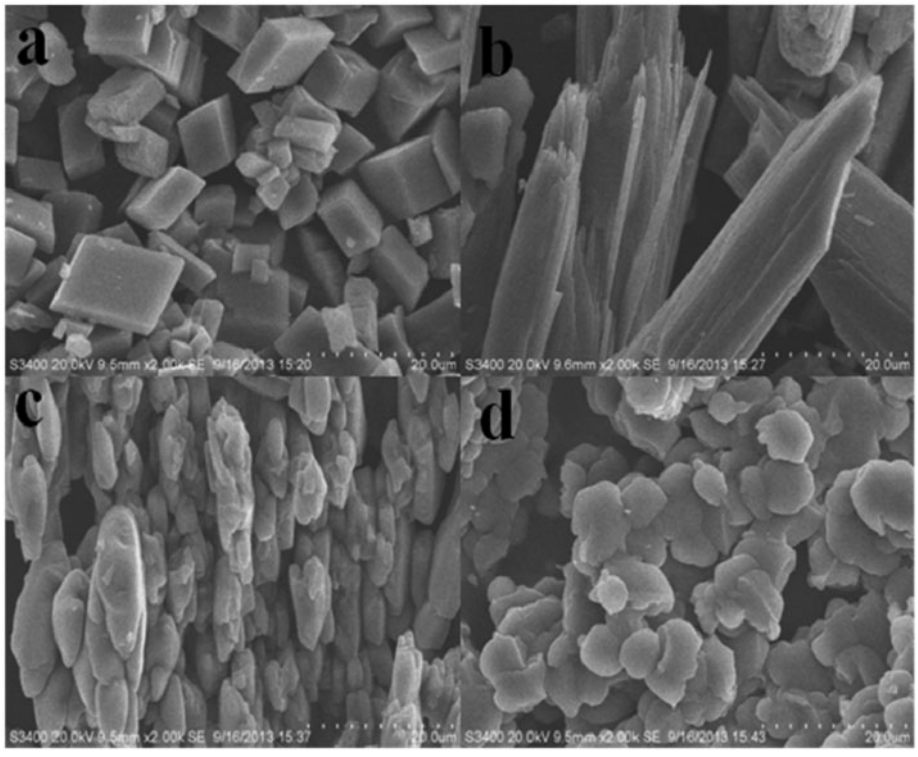

Fig. 10. SEM images for the calcium carbonate (a), with the presence of 2 mg/L (b), 6 mg/L (c), and 8 mg/L (d) AA–APEM–H_3PO_3.

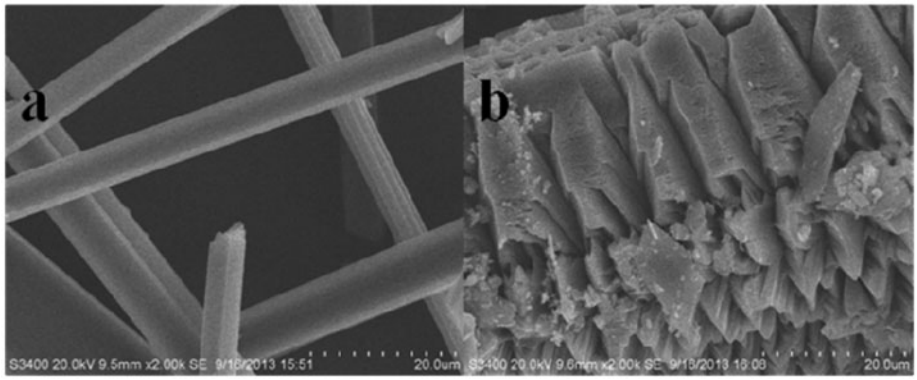

Fig. 11. SEM images for the calcium sulfate (a) and with the presence of 2 mg/L AA–APEM–H_3PO_3 (b).

absence of the low-phosphorus terpolymer, the means of XRD was used. Figs. 12 and 13 are the XRD patterns for the control as well as for a representative terpolymer system AA–APEM–H_3PO_3 of $CaCO_3$ and $CaSO_4$ scales, respectively.

It is well known that calcite is the most thermodynamically stable and vaterite the least stable form in the three polymorphic forms of $CaCO_3$ [26]. Fig. 12(a) displays that the diffraction peaks of the precipitates could be well indexed to the calcite phase of $CaCO_3$ without AA–APEM–H_3PO_3 added, including the crystal faces of (012), (104), (006), (110), (113), (202), (018), and (016). In the presence of the low-phosphorus terpolymer, the mixture of calcite, aragonite, and vaterite could be seen in Fig. 12(b), showing an agreement to that of the SEM images (Fig. 10). The crystal faces of (111), (003), and (221) are attributed to aragonite [27].

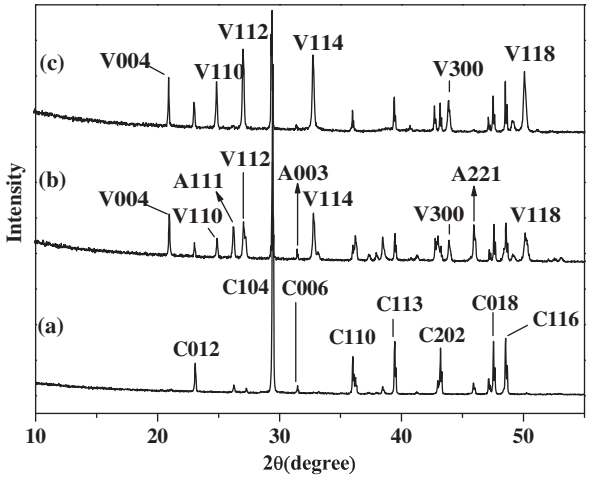

Fig. 12. The XRD pattern of the calcium carbonate crystals. (a) Without the low-phosphorus terpolymer and (b) with the low-phosphorus terpolymer.

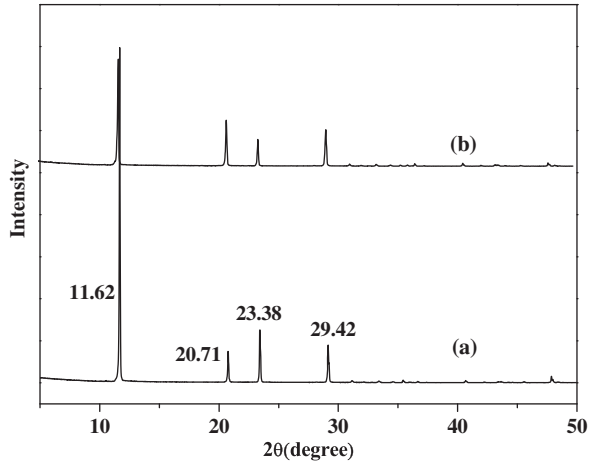

Fig. 13. The XRD pattern of the calcium sulfate crystals. (a) Without the low-phosphorus terpolymer and (b) with the low-phosphorus terpolymer.

There are the (004), (110), (112), (114), (300), and (118) strong peaks corresponding to vaterite, also weak peaks for calcite in Fig. 12(c). These results indicate that the synthesized AA–APEM–H_3PO_3 could inhibit or disturb the calcite growth and induce vaterite growth, which is harder to adhere to metal surface and easy to disperse in water solution [28].

The XRD results for sulfate crystals of calcium without and with the presence of the low-phosphorus terpolymer are presented in Fig. 13. For calcium sulfate scale, the d and θ values conform to the structure of $CaSO_4{\cdot}2H_2O$ (gypsum, calcium sulfate dihydrate, Fig. 13(a)) [5,29,30]. Fig. 13(b) illustrates that there is no change in the crystal parameters, indicating that the crystal structure is not altered with the addition of the terpolymer. Only the crystal habit or morphology is changed as evident from SEM studies.

3.5.3. FT-IR analysis of $CaCO_3$ crystals

FT-IR was used as another characterization technique to identify the various polymorphs present in the crystals. The FT-IR spectra of the calcium carbonate precipitates obtained in the absence and presence of the terpolymer are shown in Fig. 14. As shown by the curve (a), the peaks given at 874 and 712 cm^{-1} could be attributed to the vibrations of calcite [31]. In the presence of the low-phosphorus terpolymer with different concentrations, new peaks at 745 cm^{-1}, which reflect the vibrations in the vaterite form, are observed in the samples (curve (b) and (c) in Fig. 14). On the other hand, the absorption peak at 712 cm^{-1} does not disappear in the curve (b), indicating the coexistence of vaterite and calcite forms [32]. The low-phosphorus terpolymer concentration has a great influence on the FT-IR observation. As can be seen in the curve (c), there is almost no intensity of the band at 712 cm^{-1}, which means the portion of vaterite increased. All the data of the FT-IR spectra demonstrate that the terpolymer affects the polymorph of the calcium carbonate crystals.

3.6. Inhibition mechanism towards $CaCO_3$ and $CaSO_4$

The inhibitor functional groups exhibit a significant impact on the inhibitory power in terms of controlling the scale precipitation [33]. The low-phosphorus terpolymer AA–APEM–H_3PO_3 dramatically changed the morphology of the calcite and sulfate crystals, probably due to the strong specific interaction between functional groups and the crystals. In one molecule the low-phosphorus terpolymer contains –P(O)$(OH)_2$, –COOH, and PEG groups, among which both carboxylate and PEG segments are hydrophilic blocks and exist randomly in water [34]. Although $CaCO_3$ and $CaSO_4$ have limited solubility in water, they dissolve readily as they react with AA–APEM–H_3PO_3. The initial step is surface complexation of the negatively charged polydentate ligand through its carboxylate or phosphonate moieties onto the positively charged Ca^{2+} lattice ions. In fact, the phosphonate group is doubly deprotonated so that the –P(O)$(OH)_2$ moiety bridges two Ca^{2+} centers. A part of the phosphonate group and the neighboring carboxylate group oxygen atoms at the PAA segments form a seven-membered chelate with the Ca^{2+} center, while the other part chelates Ca^{2+} with several carbonyl moieties in other molecule chains [35]. As a consequence, the structure of crystals can be significantly distorted and weakened, which seems to fit the SEM images of the calcite and sulfate crystals in Figs. 8 and 9. To our knowledge, there are no structures reported of Ca^{2+} complexes that contain phosphonate/polycarboxylate/PEG ligands, indicating that the terpolymer AA–APEM–H_3PO_3 is a newly low phosphorus water treat agent.

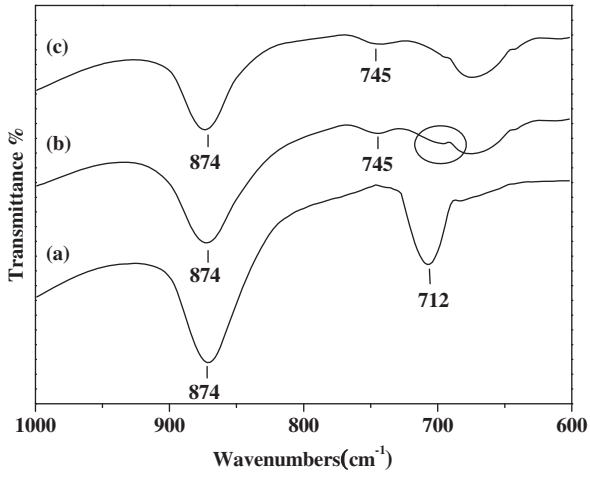

Fig. 14. FT-IR spectra of calcium carbonate precipitates. (a) In the absence of the low-phosphorus terpolymer, in the presence of (b) 2 mg/L and (c) 6 mg/L the low-phosphorus terpolymer.

4. Conclusions

In the present work, the low-phosphorus terpolymer AA–APEM–H_3PO_3 has been synthesized, characterized, and evaluated. Based on the earlier discussions, we reach the following conclusions:

(1) The phosphorus content was less than 1.5% in weight; carboxyl group, PEG group, and phosphorus group were obtained in one molecule.
(2) The results of static scale inhibition tests showed that the terpolymer is effective in the calcium scales inhibition. The terpolymer exhibited 90.16% calcium carbonate inhibition at a threshold dosage of 8 mg/L, while it exhibited 96.94% calcium sulfate inhibition at a level of 4 mg/L.
(3) The studies on calcium crystals with SEM, XRD, and FT-IR indicated that great changes in the size, morphology, and formation of the calcium scales took place under the influence of AA–APEM–H_3PO_3.
(4) The inhibition mechanism towards $CaCO_3$ and $CaSO_4$ deposits was proposed that the strong specific interaction has happened between functional groups and the calcium crystals.

No reference to the low-phosphorus terpolymer AA–APEM–H_3PO_3 used as calcium scales inhibitor in

cooling water has been found in the literature, it is believed to represent a potentially new environmental water treatment agent.

Acknowledgments

This work was supported by the Prospective Joint Research Project of Jiangsu Province (BY2012196); the National Natural Science Foundation of China (51077013); special funds for Jiangsu Province Scientific and Technological Achievements Projects of China (BA2011086); the Fundamental Research Funds for the Central Universities; Scientific Innovation Research Foundation of College Graduate in Jiangsu Province (CXLX13-107); program for Training of 333 High-Level Talent, Jiangsu Province of China (BRA2010033).

References

[1] D.E. Abd-El-Khalek, B.A. Abd-El-Nabey, Evaluation of sodium hexametaphosphate as scale and corrosion inhibitor in cooling water using electrochemical techniques, Desalination 311 (2013) 227–233.
[2] A.L. Kavitha, T. Vasudevan, H.G. Prabu, Evaluation of synthesized antiscalants for cooling water system application, Desalination 268 (2011) 38–45.
[3] C. Wang, S.P. Li, T.D. Li, Calcium carbonate inhibition by a phosphonate-terminated poly(maleic-co-sulfonate) polymeric inhibitor, Desalination 249 (2009) 1–4.
[4] Z.H. Shen, J.S. Li, K. Xu, L.L. Ding, The effect of synthesized hydrolyzed polymaleic anhydride (HPMA) on the crystal of calcium carbonate, Desalination 284 (2012) 238–244.
[5] P. Shakkthivel, T. Vasudevan, Acrylic acid-diphenylamine sulphonic acid copolymer threshold inhibitor for sulphate and carbonate scales in cooling water systems, Desalination 197 (2006) 179–189.
[6] J.G. Knudsen, Fouling in Heat Exchangers, Hemisphere Handbook of Heat Exchanger Design, Hemisphere, Washington, DC, 1990.
[7] C. Gabrielli, G. Maurin, H. Perrot, G. Poindessous, R. Rosset, Investigation of electrochemical calcareous scaling: Potentiostatic current- and mass-time transients, J. Electroanal. Chem. 538–539 (2002) 133–143.
[8] M. Öner, Ö. Doğan, G. Öner, The influence of polyelectrolytes architecture on calcium sulfate dihydrate growth retardation, J. Cryst. Growth 186 (1998) 427–437.
[9] E. Akyol, M. Öner, E. Barouda, K.D. Demadis, Systematic structural determinants of the effects of tetraphosphonates on gypsum crystallization, Cryst. Growth Des. 9 (2009) 5145–5154.
[10] X.X. Xue, C.E. Fu, N. Li, F.F. Zheng, W.B. Yang, X.D. Yang, Performance of a non-phosphorus antiscalant on inhibition of calcium-sulfate precipitation, Water Sci. Tech. 66 (2012) 193–200.
[11] B. Nowack, Environmental chemistry of phosphonates, Water Res. 37 (2003) 2533–2546.
[12] Y.M. Tang, W.Z. Yang, X.S. Yin, Y. Liu, P.W. Yin, J.T. Wang, Investigation of $CaCO_3$ scale inhibition by PAA, ATMP and PAPEMP, Desalination 228 (2008) 55–60.
[13] K.D. Demadis, S.D. Katarachia, M. Koutmos, Crystal growth and characterization of zinc–(amino-tris-(methylenephosphonate)) organic–inorganic hybrid networks and their inhibiting effect on metallic corrosion, Inorg. Chem. Commun. 8 (2005) 254–258.
[14] K.D. Demadis, P. Baran, Chemistry of organophosphonate scale growth inhibitors: Two-dimensional, layered polymeric networks in the structure of tetrasodium 2-hydroxyethyl-amino-bis(methylenephosphonate), J. Solid State Chem. 177 (2004) 4768–4776.
[15] A. Tsortos, G.H. Nancollas, The role of polycarboxylic acids in calcium phosphate mineralization, J. Colloid Interface Sci. 250 (2002) 159–167.
[16] Z. Amjad, Influence of polyelectrolytes on the precipitation of amorphous calcium phosphate, Colloid. Surf. 48 (1990) 95–106.
[17] S. Lattemann, T. Höpner, Environmental impact and impact assessment of seawater desalination, Desalination 220 (2008) 1–15.
[18] D. Hasson, H. Shemer, A. Sher, State of the art of friendly "green" scale control inhibitors: A review article, Ind. Eng. Chem. Res. 50 (2011) 7601–7607.
[19] A.A. Koelmans, H.A. Vander, L.M. Knijff, Integrated modelling of eutrophication and organic contaminant fate & effects in aquatic ecosystems. A review, Water Res. 35 (2001) 3517–3536.
[20] K. Du, Y.M. Zhou, L Wang, Fluorescent-tagged no phosphate and nitrogen free calcium phosphate scale inhibitor for cooling water systems, J. Appl. Poly. Sci. 113 (2009) 1966–1974.
[21] G.Q. Liu, J.Y. Huang, Y.M. Zhou, Q.Z. Yao, L. Ling, P.X. Zhang, H.C. Wang, K. Cao, Y.H. Liu, W.D. Wu, W. Sun, Z.J. Hu, Fluorescent-tagged double-hydrophilic block copolymer as a green inhibitor for calcium carbonate scales, Tenside Surf. Det. 49 (2012) 404–412.
[22] C.E. Fu, Y.M. Zhou, J.Y. Huang, H.T. Xie, G.Q. Liu, W.D. Wu, Control of iron(III) scaling in industrial cooling water systems by the use of maleic anhydride-ammonium allylpolyethoxy sulphate dispersant, Adsorpt. Sci. Technol. 28 (2010) 437–448.
[23] G. Nehrke, P. Van Cappellen, Framboidal vaterite aggregates and their transformation into calcite: A morphological study, J. Cryst. Growth 287 (2006) 528–530.
[24] G.L. Jing, X.X. Li, Dynamic laboratory research on synergistic scale inhibition effect of composite scale inhibitor and efficient electromagnetic anti-scaling instrument, Appl. Sci. Eng. Technol. 6 (2013) 3372–3377.
[25] Z. Amjad, Calcium sulfate dihydrate (gypsum) scale formation on heat exchanger surfaces: The influence of scale inhibitors, J. Colloid Interface Sci. 123 (1988) 523–536.
[26] A.G. Xyla, J. Mikroyannidis, P.G. Koutsoukos, The inhibition of calcium carbonate precipitation in aqueous media by organophosphorus compounds, J. Colloid Interface Sci. 153 (1992) 537–551.
[27] M.Z. Xia, F.Y. Wang, W. Lei, S.G. Zhang, Scale-inhibiting mechanism of phosphono carboxylic acid on $CaCO_3$, J. Chem. Ind. Eng. 59 (2008) 982–987 (in Chinese).
[28] T. Chen, A. Neville, K. Sorbie, Z. Zhong, In-situ monitoring the inhibiting effect of polyphosphinocarboxylic acid on $CaCO_3$ scale formation by synchrotron X-ray diffraction, Chem. Eng. Sci. 64 (2009) 912–918.

[29] H.A. El Dahan, H.S. Hegazy, Gypsum scale control by phosphate ester, Desalination 127 (2000) 111–118.
[30] P. Shakkthivel, D. Ramesh, R. Sathiyamoorthi, T. Vasudevan, Water soluble copolymers for calcium carbonate and calcium sulphate scale control in cooling water systems, J. Appl. Polym. Sci. 96 (2005) 1451–1459.
[31] N. Ueyama, T. Hosoi, Y. Yamada, M. Doi, T. Okamura, A. Nakamura, Calcium complexes of carboxylate-containing polyamide with sterically disposed NH···O hydrogen bond: Detection of the polyamide in calcium carbonate by 13C cross-polarization/magic angle spinning spectra, Macromolecules 31(21) (1998) 7119–7126.
[32] S. Kirboga, M. Oner, Investigation of calcium carbonate precipitation in the presence of carboxymethyl inulin, Royal. Soc. Chem. 15 (2013) 3678–3686.
[33] C.E. Fu, Y.M. Zhou, H.T. Xie, Double-hydrophilic block copolymers as precipitation inhibitors for calcium phosphate and Iron (III), Ind. Eng. Chem. Res. 49 (2010) 8920–8926.
[34] C.E. Fu, Y.M. Zhou, G.Q. Liu, J.Y. Huang, W. Sun, W.D. Wu, Inhibition of $Ca_3(PO_4)_2$, $CaCO_3$, and $CaSO_4$ precipitation for industrial recycling water, Ind. Eng. Chem. Res. 50 (2011) 10393–10399.
[35] K.D. Demadis, P. Lykoudis, R.G. Raptis, G. Mezei, Phosphonopolycarboxylates as chemical additives for calcite scale dissolution and metallic corrosion inhibition based on a calcium-phosphonotricarboxylate organic−inorganic hybrid, Cryst. Growth Des. 6 (2006) 1064–1067.